Astron. Astrophys. 209, 349–360 (1989)

ASTRONOMY AND ASTROPHYSICS

Large-scale behaviour of dust grains in a galactic environment

B. Barsella[1], **F. Ferrini**[1], **J.M. Greenberg**[2], **and S. Aiello**[3]

[1] Istituto di Astronomia, Università di Pisa, piazza Torricelli 2, I-56100 Pisa, Italy
[2] Laboratory Astrophysics, University of Leiden, Huygens Laboratorium, Postbus 9504, NL-2300 RA Leiden, The Netherlands
[3] Dipartimento di Fisica, Università di Firenze, via Pancaldo 3/45, I-50127 Firenze, Italy

Received December 9, 1987; accepted July 18, 1988

Summary. The extensive forces on dust grains subjected to the light and matter distribution of a spiral galaxy are considered. The combined force on a small particle located above the plane of a galactic disk may be either attractive or repulsive depending on a variety of parameters. We find that graphite grains from 20 nm to 250 nm radius are expelled from a typical galaxy, while silicates and other forms of dielectrics, after initial expulsion, may settle in a potential minimum within the halo. We discuss only the static behaviour of the forces, with the sole exception of the drag force due to the gas. The detectability of such external dust distributions above and below spiral galaxies seen edge-on is considered. Some cosmological and observational consequences of a differential ejection of one grain species relative to the others are noted.

Key words: interstellar medium: dust – intergalactic medium – galaxies: haloes of

1. Introduction

Dust is now recognized to be a fundamental component of the galaxy on all length scales; from local dense clouds to molecular cloud concentrations, accompanying OB associations to fully global distributions. Indeed the IRAS observations at 100 μm revealed that, in the Milky Way, dust is distributed very similarly to the H I component (Burton, 1986). Furthermore, intergalactic extinction, due to both a diffuse medium and individual clouds (Rudnicki, 1986) is a subject of renewed interest, because of its connection with cosmological observations and theories.

While there exists a rich investment in the observational aspects of dust distributions, only incidental interest has been focused on the theoretical study of the forces which act on grains, with the exception of those in the interplanetary medium. For example, no accurate model of the dust distribution in OB associations has been published, although one can easily imagine that grains will wind up in sponge-like configurations, with hot stars at the center of large haloes (Shin and Hong, 1987). We note incidentally that this characteristic distribution may have a certain relevance to the fact that stars in the same associations may have different extinction curves: this effect may be due to the inhomogeneity of obscuring material along the line of sight inside the association.

Send offprint requests to: B. Barsella

A few papers (Pecker, 1972, 1974; Chiao and Wickramasinghe, 1972) have considered the relatively simple problem of the forces on dust grains due to essentially continuous distributions of light and matter like the ones in the disk and halo of a spiral galaxy. The present authors have already presented (Greenberg et al. 1987) some preliminary results of the detailed analysis of the forces exerted by a galaxy on dust grains with different optical properties. This will be further amplified in this paper. The motion of grains, considered as test particles in the luminous and gravitational fields of the galaxy, depends on a convolution of the galactic properties and the grain properties. It turns out that the effects of a massive halo will be important.

The optical properties of the interstellar grains we consider are described in Sect. 2. We then formalize the force expression (Sect. 3) and choose a model galaxy (Sect. 4). Before presenting the numerical results of our model (Sect. 7), we demonstrate analytically that equilibrium positions in the halo are possible for silicate grains (Sect. 5) and provide some arguments about possible observations to demonstrate this peculiar behaviour of dust (Sect. 6). We conclude by comparing our results with earlier ones. We also demonstrate some cosmological consequences of our analysis (Sect. 8).

2. Grain optics

The basic parameters required to calculate the grain forces are the optical properties, the sizes and the densities.

The principal populations of interstellar grains that we consider may be divided optically into two categories: dielectric and metallic. The dielectric grains are represented by either silicate core-organic refractory mantles or by pure silicate grains. In the trimodal model (Hong and Greenberg, 1980; Greenberg and Chlewicki, 1983), the core-mantle grains have a mean overall size (as represented by spheres) of $a \simeq 0.15$ μm. In the MRN (silicates + graphite) model (Mathis et al., 1977) the silicates are characterized by about the same size, because in both models these grains are responsible for the optical polarization.

Metallic grains in both models are represented by graphite, although there are considerable problems in justifying this material in space: in the Greenberg–Chlewicki model the "graphite" is restricted to very small ($a < 0.01$ μm) sizes, whereas in the MRN model a wide range of sizes up to tenth micron particles is included in the distribution.

To cover the full spectrum of possibilities, we have considered scattering by dielectric particles from 5 nm to 250 nm radius (the lower limit being dictated by applicability of the standard Mie theory electromagnetic scattering formulation). These limits have also been used for the metallic particles. All particles will be represented by spheres.

The optical properties of the core-mantle particles should not be qualitatively different from the silicates and as the optical properties of organic refractory materials become available, we will extend our calculations to them. For the moment, it is convenient to use the available Draine and Lee (1984) "astronomical silicate" properties as representative of the dielectrics.

The graphite optical constants are taken from Tosatti and Bassani (1970) for the parallel graphite and from Phillip (1977 and private communication) for the perpendicular graphite.

In calculating radiation pressure forces in the galactic environment we assume that this force is continuous even though, in a tenuous radiation field, the impulses will be sporadic – particularly for the ultraviolet photons. The stochastic effects will be incorporated in a future publication.

We restrict ourselves to estimating the gravitational and radiation pressure forces on a spherical solid grain of radius betwen 5 nm and 250 nm, disregarding possible mantles of ice or organic material.

For the gravitational force the problem is extremely easy: the force on a grain of mass m_g may be written:

$$\boldsymbol{F}_G(\boldsymbol{r}) = m_g \boldsymbol{G}(\boldsymbol{r}), \tag{1}$$

where $\boldsymbol{G}(\boldsymbol{r})$ is the gravitational field intensity at the point $\boldsymbol{r}$.

The formula for the radiation pressure force is more complicated, being an integral over the radiation frequency dependent $Q_{\rm pr}$:

$$\boldsymbol{F}_R(\boldsymbol{r}) = \pi a^2 \int d\boldsymbol{\rho} \int d\nu Q_{\rm pr}(a,\nu) \boldsymbol{\Psi}(\boldsymbol{r},\boldsymbol{\rho},\nu), \tag{2}$$

where $Q_{\rm pr}(a,\nu)$ is the radiation pressure coefficient for a grain of radius a at frequency ν, $\boldsymbol{\Psi}$ is the radiation field due to the galactic element at $\boldsymbol{\rho}$ on the grain at position $\boldsymbol{r}$ at frequency ν.

In this paper and for a typical galactic component (disk + halo), the wavelength dependence of the luminosity is assumed independent of the position. Therefore, the radiation field function may be written:

$$\boldsymbol{\Psi}(\boldsymbol{r},\boldsymbol{\rho},\nu) = \boldsymbol{\Xi}(\boldsymbol{r},\boldsymbol{\rho})\Omega(\nu)$$

and the integration over ν in (2) yields the formulae:

$$Q^*_{\rm pr}(a) = \int d\nu Q_{\rm pr}(a,\nu)\Omega(\nu) \tag{3a}$$

$$\boldsymbol{F}_R(\boldsymbol{r}) = \pi a^2 Q^*_{\rm pr}(a) \int d\boldsymbol{\rho}\, \boldsymbol{\Xi}(\boldsymbol{r},\boldsymbol{\rho}) = \pi a^2 Q^*_{\rm pr}(a)\boldsymbol{\Gamma}(\boldsymbol{r}). \tag{3b}$$

The expression for the radiation pressure force is reduced, therefore, to a form similar to the formula for the gravitational force.

To perform the integration of (3a), it is necessary to know the frequency dependence of the galactic disk (or bulge) luminosity for a model galaxy. Since these data are not widely known, we have decided to take a simplified point of view, and to model this frequency dependence with a black body function at a temperature T_0; i.e. $\Omega(\nu) = B_\nu(T_0)$ for which $Q^*_{\rm pr}(a) \equiv Q_{\rm pr}(a, T_0)$.

The calculation of $Q_{\rm pr}(a, T_0)$ has, therefore, been made for a set of temperatures, where the radiation pressure coefficients depend not only on the grain radius but also on the galactic disk temperature.

Table 1 gives an example of the values of $Q_{\rm pr}$ used in this work.

Table 1. $Q_{\rm pr}(a, T_0)$ for graphite (g) and astronomical silicate (s), as a function of a (nanometers) and T_0 (degrees Kelvin)

$T_0 =$ a	6000 g	6000 s	9000 g	9000 s	12000 g	12000 s
10	0.11525	0.00101	0.22416	0.00904	0.32002	0.03802
20	0.25595	0.00457	0.50497	0.03615	0.72053	0.13233
50	0.93019	0.07675	1.48570	0.28752	1.75736	0.58755
100	1.90756	0.38304	2.09411	0.79102	2.04601	1.10546
150	2.17217	0.70375	2.06829	1.08951	1.91631	1.29218
200	2.14684	0.93719	1.93986	1.22583	1.77319	1.33146
250	2.05097	1.08566	1.81920	1.27220	1.66084	1.31371

3. The forces on the grain

A dust grain in a spiral galaxy is subjected to effects of both the light and matter distribution. In this section, we analyze the forces on a dust grain located outside or near the edge of the galactic disk.

Since we are only interested in the large scale distribution of dust grains, we shall not include any local effects such as those associated with young stellar phases, e.g., winds and outflows from young stars and inflows caused by gravitational accretion on young and old objects. These phenomena will only contribute to a stochastic distribution of initial velocities to the grains. The geometry of the galaxy is described in Fig. 1. The contributions to the light and mass distributions of a spiral galaxy come from three components: disk, bulge and halo. We assume that the bulge and halo components have spherical symmetry; the disk will be considered axially symmetric, so that the expression for the forces may be limited to the y, z plane.

The surface light distribution of the disk is $I(\rho)$ and the dependence on the frequency has been eliminated by integration of $Q_{\rm pr}$ over a black body spectrum, as described in Sect. 2.

The total force exerted by the light coming from the disk (assumed as thin), is

$$\boldsymbol{F}_{\rm rad,\,disk} = \frac{\pi a^2 Q_{\rm pr}}{c} \int_0^{2\pi} \int_0^{R_L} I(\rho) \frac{\boldsymbol{r}-\boldsymbol{\rho}}{|\boldsymbol{r}-\boldsymbol{\rho}|^3} d\phi \rho d\rho \tag{4}$$

where R_L is the radius to which the light distribution extends.

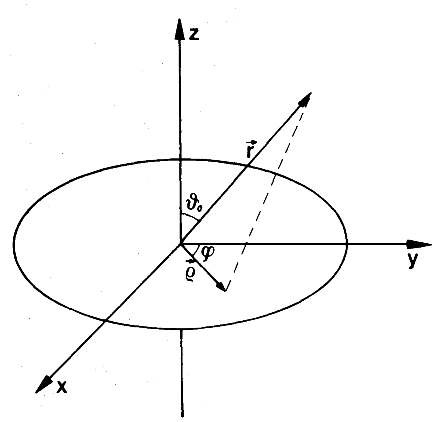

Fig. 1. Geometry of the galactic model. The galactic disk is in the x–y plane

Projecting the force on the axes of Fig. 1 we have:

$$F_{\mathrm{rad,disk},y} = \frac{\pi a^2 Q_{\mathrm{pr}}}{c}\int_0^{2\pi} d\phi \int_0^{R_L} I(\rho)\frac{(r\sin\theta_0-\rho\cos\phi)\rho d\rho}{(r^2+\rho^2-2r\rho\sin\theta_0\cos\phi)^{3/2}}$$

$$F_{\mathrm{rad,disk},z} = \frac{\pi a^2 Q_{\mathrm{pr}}}{c}\int_0^{2\pi} d\phi \int_0^{R_L} I(\rho)\frac{r\cos\theta_0\,\rho d\rho}{(r^2+\rho^2-2r\rho\sin\theta_0\cos\phi)^{3/2}}. \quad (5)$$

Introducing the nondimensional variables $\xi=\rho/R_L$ and $\Delta=r/R_L$, the above expressions become:

$$F_{\mathrm{rad,disk},y} = \frac{\pi a^2 Q_{\mathrm{pr}}}{c}\left[\Delta\sin\theta_0\int_0^{2\pi} d\phi\int_0^1 I(\xi R_L)\frac{\xi d\xi}{(\Delta^2+\xi^2-2\xi\Delta\sin\theta_0\cos\phi)^{3/2}} - \int_0^{2\pi}\cos\phi d\phi\int_0^1 I(\xi R_L)\frac{\xi^2 d\xi}{(\Delta^2+\xi^2-2\xi\Delta\sin\theta_0\cos\phi)^{3/2}}\right] \quad (6)$$

$$F_{\mathrm{rad,disk},z} = \frac{\pi a^2 Q_{\mathrm{pr}}}{c}\Delta\cos\theta_0 \int_0^{2\pi} d\phi\int_0^1 I(\xi R_L)\frac{\xi d\xi}{(\Delta^2+\xi^2-2\xi\Delta\sin\theta_0\cos\phi)^{3/2}}.$$

A bulge with luminosity L_b contributes a force acting on a grain of

$$F_{\mathrm{rad,bulge},y} = \frac{\pi a^2 Q_{\mathrm{pr,b}}}{c}\frac{L_b}{4\pi r^2}\sin\theta_0$$

$$F_{\mathrm{rad,bulge},z} = \frac{\pi a^2 Q_{\mathrm{pr,b}}}{c}\frac{L_b}{4\pi r^2}\cos\theta_0, \quad (7)$$

where we indicate with $Q_{\mathrm{pr,b}}$ the radiation pressure cross section corresponding to the bulge temperature, which in general is different from the effective temperature of the disk. The bulge and disk stellar populations are different, because they have had a different star formation history.

The luminosity contribution of the halo stars may be considered completely negligible. This, together with the assumption that the integrated light distribution of the disk is seen by the grains as flat, are the only simplifying hypotheses we make for the radiation force; both assumptions are indeed very good approximations.

The gravitational force is similarly produced by the disk, bulge and halo. An axially symmetric flat disk with surface density $\sigma(\rho)$ exercises the following force on a grain of radius a and density δ_g:

$$F_{\mathrm{grav,disk},y} = -\frac{4}{3}\pi a^3 G\delta_g\int_0^{2\pi} d\phi\int_0^{R_M} \times\sigma(\rho)\frac{(r\sin\theta_0-\rho\cos\phi)\rho d\rho}{(r^2+\rho^2-2r\rho\sin\theta_0\cos\phi)^{3/2}}$$

$$F_{\mathrm{grav,disk},z} = -\frac{4}{3}\pi a^3 G\delta_g\int_0^{2\pi} d\phi\int_0^{R_M} \times\sigma(\rho)\frac{r\cos\theta_0\,\rho d\rho}{(r^2+\rho^2-2r\rho\sin\theta_0\cos\phi)^{3/2}}, \quad (8)$$

where R_M is the radius of the mass distribution. Defining the nondimensional variables $\zeta=\rho/R_M$, $\Phi=r/R_M$, we may write:

$$F_{\mathrm{grav,disk},y} = -\frac{4}{3}\pi a^3 G\delta_g \times\left[\Phi\sin\theta_0\int_0^{2\pi} d\phi\int_0^1\sigma(\zeta R_M)\frac{\zeta d\zeta}{(\Phi^2+\zeta^2-2\zeta\Phi\sin\theta_0\cos\phi)^{3/2}} - \int_0^{2\pi}\cos\phi d\phi\int_0^1\sigma(\zeta R_M)\frac{\zeta^2 d\zeta}{(\Phi^2+\zeta^2-2\zeta\Phi\sin\theta_0\cos\phi)^{3/2}}\right] \quad (9)$$

$$F_{\mathrm{grav,disk},z} = -\frac{4}{3}\pi a^3 G\delta_g\Phi\cos\theta_0 \int_0^{2\pi} d\phi\int_0^1\sigma(\zeta R_M)\frac{\zeta d\zeta}{(\Phi^2+\zeta^2-2\zeta\Phi\sin\theta_0\cos\phi)^{3/2}}.$$

At a distance r, larger than its radius, the bulge with mass M_b will exert a force

$$F_{\mathrm{grav,bulge},y} = -\frac{4}{3}\pi a^3 G\delta_g\frac{M_g\sin\theta_0}{r^2}$$

$$F_{\mathrm{grav,bulge},z} = -\frac{4}{3}\pi a^3 G\delta_g\frac{M_b\cos\theta_0}{r^2}. \quad (10)$$

The mass distribution M(r) of the halo results in a central force:

$$F_{\mathrm{grav,halo},y} = -\frac{4}{3}\pi a^3 G\delta_g\frac{M(r)\sin\theta_0}{r^2}$$

$$F_{\mathrm{grav,halo},z} = -\frac{4}{3}\pi a^3 G\delta_g\frac{M(r)\cos\theta_0}{r^2}. \quad (11)$$

We see that the spatial structure of the total force coming from all these components may be rather complex and could perhaps have an interesting and not obvious behaviour.

Before applying the results of the combined gravitational and radiation pressure forces calculated in the next sections on the dust motion, we shall first consider the possible modifying effects due to other forces, that is gas drag, Poynting-Robertson and Lorentz forces.

3.1. Gas drag

A reasonable way to evaluate the effect of the gas drag on the motion of dust grains is to make a direct comparison of the drag force with the gravitational and radiative force acting on the grain.

Let us take the following expression for the force exerted by the gas

$$F_{\mathrm{gas}} = 4\pi a^2 nkT\frac{u_{\mathrm{grain}}}{v}$$

where u_{grain} is the grain velocity, v is the thermal velocity of the gas, and n its number density. This expression is valid (see e.g. Chiao and Wickramasinghe, 1972) in the limit $u_{\mathrm{grain}} \ll v$.

This condition is well satisfied in the regions near the plane of the disk; the typical velocity acquired by the grain due to the forces evaluated in Sect. 3, in the interval of two subsequent collisions with atoms, is lower than $10^{-2}\,\mathrm{km\,s^{-1}}$, while the typical thermal velocities of the gas are larger than $0.1\,\mathrm{km\,s^{-1}}$.

The radiative and gravitational force is, from Eq. (14):

$$F = Gm_g\frac{M_\odot}{pc^2}H,$$

where by H we indicate the nondimensional factor in Eq. (14). The condition of expulsion ($F > F_{gas}$) gives, for a "typical" grain with $\delta = 3.3$ and $a_{nm} = 100$:

$$H > 10^{-4} n \sqrt{T u_{grain}} .$$

The worst condition will be $u_{grain} = v$, that is

$$H > nT .$$

In Fig. 2, we show, in the plane $\log n$–$\log T$, the regions occupied by the interstellar medium, whose components are described according to Mihalas and Binney (1981), Güsten and Metzger (1983) and Shull (1987). The lines correspond to different values of the product nT.

The typical values of H, 80–150 pc above the galactic plane and at different distances ρ from the galactic center, are:

ρ (kpc)	0	5	10	15
H:	$2\,10^4$	$4.5\,10^3$	$3\,10^3$	$7\,10^2$

The volume filling factors and the mass fractions of the various phases are, respectively:

		Filling factor	Mass fraction
MC	molecular clouds	0.01	≈ 0.9
CM	cold medium	$\approx 0.02 \div 0.04$	
WNM	warm neutral medium	≈ 0.2	≈ 0.05
WIM	warm ionized medium	≈ 0.2	≈ 0.05
HIM	hot ionized medium	≈ 0.06	$\approx 10^{-3}$

As a conclusion, it is possible to classify the different galactic phases according to their permissivity for grain expulsion. A good classifying parameter, after our previous considerations, is

$$R = H/nT .$$

A high value of this parameter characterizes the regions where the drag force of the gas is not sufficient to confine the grains for a long period of time. As an example, at a distance $\rho = 5$ kpc, R has the following typical values for the various phases:

MC	CM	WNM	WIM	HIM
≈ 0.25	≈ 2.25	≈ 1	≈ 3	≈ 4.5

It results therefore that the interaction with the gas is predominant in the dense cloud phase, is important in all regions to limit the grain escape velocity and is negligible only in the halo region outside the disk.

A more complete discussion of the gas drag force will be given in a following paper concerning the dynamical analysis of the grain motions.

3.2. Poynting–Robertson force

The Poynting–Robertson force comes from the fact that a grain reemits isotropically the absorbed electromagnetic radiation in a system of reference at velocity $\boldsymbol{v}$ with respect to the light emitting galaxy. This force has been discussed exhaustively in relation to interplanetary particles, where its effect is extremely important;

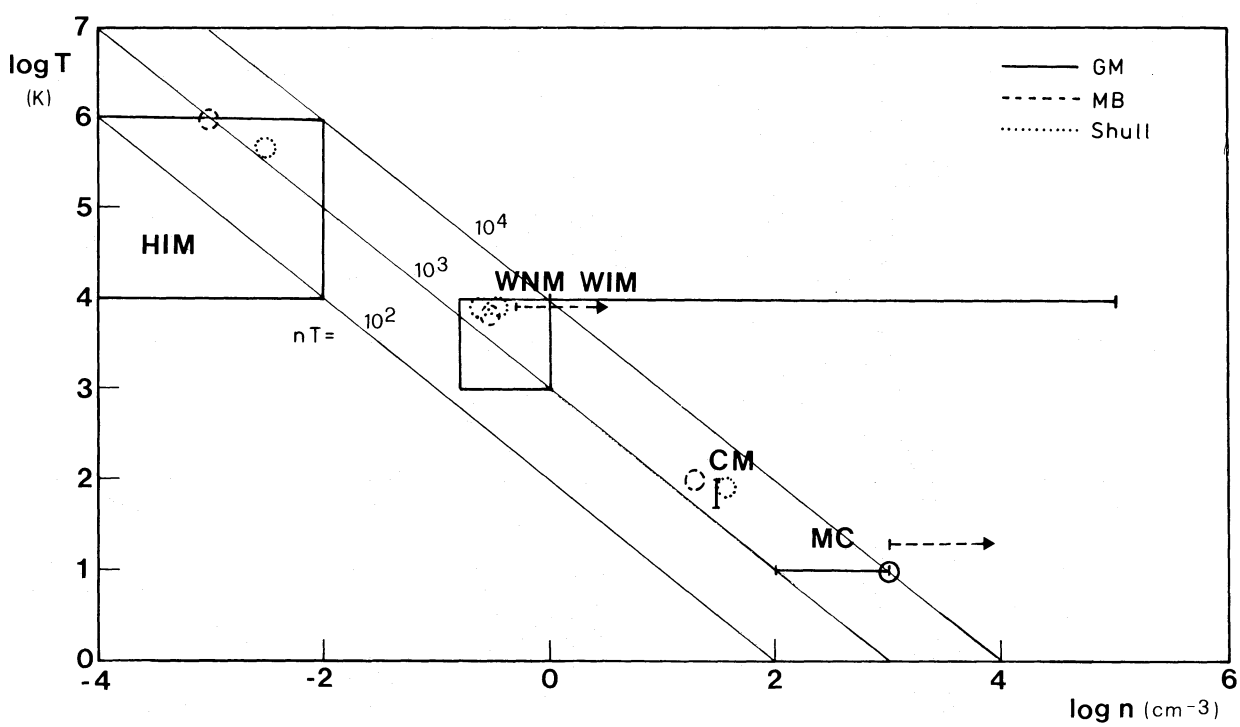

Fig. 2. Regions occupied by the interstellar medium, after Mihalas and Binney (1981), Güsten and Metzger (1983) and Shull (1987). The lines correspond to different values of the product nT

see, for example, the paper by Burns, et al. (1979). The value of the PR force is:

$$F_{PR} = -K_{pr}\frac{v}{c}$$

where K_{pr} is the galactic radiation pressure force. Since the velocity of the grain may reasonably attain at most a value of 300–400 km s^{-1}, the Poynting–Robertson force is at most one thousandth of the main force. We therefore disregard it completely, for the moment. A possible relevance could exist in a discussion of the dynamical behaviour of the grain distribution.

3.3. *Lorentz force*

The Lorentz force on charged grains has greater significance for two reasons: 1) a grain in the disk environment is readily charged by either ultraviolet photons or by grain or atom collisions (see Draine and Salpeter, 1979) and 2) in some places in the disk the magnetic field is strong enough to confine a 1 km s^{-1} singly-charged grain in a space of a few parsecs around the lines of the magnetic field. In this work, we have disregarded the magnetic force for two reasons. First, in actuality the Lorentz force is sporadic, turning off when the grain loses its charge. Since the mean charge on a grain is significantly less than unity in the halo environment, the grain is generally subjected to the radiation pressure and gravitational forces alone and only sporadically does it spiral around magnetic field lines. In this environment, the magnetic field is not known, but it is in general less than in the arms, and distributed chaotically so that the net effect is a slight increase in the time scale for the effects of the gravitation and radiation pressure motion. Second, observations by IRAS show that dust grains are not confined to the arms, in our galaxy, but that they also spread into the H I interarm zone. There is therefore evidence that "strong" magnetic field confinement is not everywhere effective.

4. A model galaxy

To obtain quantitative results for the effect we are seeking, we must choose a model galaxy for which the luminosity and matter distribution are reasonably well known. We require a galaxy for which extended observations have been done, including optical mapping for the luminosity profile and radio mapping for the rotation curve of hydrogen at large radii. This excludes our own Milky Way. A spiral galaxy for which detailed distributions have been published is NGC 3198. In a future paper, we will give a more general set of calculations, to study the dependence of the results on galaxy modelling.

In general, the light distribution of many spiral galaxies is well established, while the mass distribution of its components is not so well known, particularly the mass in the halo. We will consider NGC 3198 in the following example.

We use Wevers' (1984) light distributions. The radial luminosity profile is fitted by an exponential disk, excluding the presence of a bulge. The expression we adopt is $I(\rho) = I_0 e^{-\lambda\rho}$, where $I_0 = 190\,L_\odot\,\mathrm{pc}^{-2}$, the exponential scale is $\lambda^{-1} = 2.68$ kpc, the luminosity radius $R_L = 18$ kpc. The total blue luminosity is $L_B = 8.6\,10^9\,L_\odot$. For the bulge we have $L_b = 0$.

As far as the mass distribution is concerned, we refer to van Albada et al. (1985). We take the 'maximum disk' case for their two component model: thin disk plus spheroidal halo (the bulge is not relevant, so we assume $M_b = 0$). The disk mass distribution is $\sigma(\rho) = \sigma_0 e^{-\lambda\rho}$, where $\sigma_0 = 687\,M_\odot\,\mathrm{pc}^{-2}$, the exponential scale is the same as the luminosity one $\lambda^{-1} = 2.68$ kpc, the extention of the mass distribution is $R_M = 50$ kpc, and the total mass of the disk is $3.1\,10^{10}\,M_\odot$.

The mass of the halo is given by

$$M(r) = 7.14\,10^{10}\,M_\odot \int_0^{r/R_0} \frac{x^2\,dx}{1.5625 + x^2 + 0.08x^4}, \tag{12}$$

where $R_0 = 8$ kpc, or equivalently

$$M(r) = [3.298 \arctan(0.038r) - 1.338 \arctan(0.092r)] \times 10^{11}\,M_\odot.$$

$$(r \text{ in kpc}). \tag{13}$$

In support of our choice of NGC 3198 as a model galaxy, Burstein and Rubin (1985) note in their study that its "integral mass distribution matches that of other galaxies", independently of the presence of a massive bulge. Furthermore, its mass profile corresponds to the intermediate one (type II in their terminology), justifying our assumption that this is not only a well known, but also a reasonably typical galaxy.

5. Simple analytical arguments to prove the confinement of dust grains

Let us analyze the expression for the components of total force on a grain of mass m_g in the y and z directions:

$$F_y = Gm_g \frac{M_\odot}{\mathrm{pc}^2}\left[7215\frac{Q_{pr}}{a_{nm}\delta}(I_0 \Delta f_1 \sin\theta_0 - I_0 f_2) - \left(\sigma_0 \Phi g_1 \sin\theta_0 - \sigma_0 g_2 + \frac{M(r)}{r^2}\sin\theta_0\right)\right] \tag{14}$$

$$F_z = Gm_g \frac{M_\odot}{\mathrm{pc}^2}\left[7215\frac{Q_{pr}}{a_{nm}\delta} I_0 \Delta f_1 - \left(\sigma_0 \Phi g_1 + \frac{M(r)}{r^2}\right)\right]\cos\theta_0,$$

where r is measured in kpc, a_{nm} is in nanometers, δ is the specific density, $M(r)$ is in units of $10^6\,M_\odot$, and where the quantities f_1, f_2, g_1 and g_2 are given by the following integrals

$$f_1 = \int_0^{2\pi} d\phi \int_0^1 e^{-\lambda R_L \xi} \frac{\xi\,d\xi}{(\Delta^2 + \xi^2 - 2\xi\Delta \sin\theta_0 \cos\phi)^{3/2}}$$

$$f_2 = \int_0^{2\pi} \cos\phi\,d\phi \int_0^1 e^{-\lambda R_L \xi} \frac{\xi\,d\xi}{(\Delta^2 + \xi^2 - 2\xi\Delta \sin\theta_0 \cos\phi)^{3/2}} \tag{15}$$

$$g_1 = \int_0^{2\pi} d\phi \int_0^1 e^{-\lambda R_M \zeta} \frac{\zeta\,d\zeta}{(\Phi^2 + \zeta^2 - 2\zeta\Phi \sin\theta_0 \cos\phi)^{3/2}}$$

$$g_2 = \int_0^{2\pi} \cos\phi\,d\phi \int_0^1 e^{-\lambda R_M \zeta} \frac{\zeta^2\,d\zeta}{(\Phi^2 + \zeta^2 - 2\zeta\Phi \sin\theta_0 \cos\phi)^{3/2}}. \tag{16}$$

The integrand in f_1 is the product of an exponential and another function, whose typical behaviour is given in Fig. 3. The product of the two is the solid line in the same figure. The maximum occurs approximately where the two curves are equal. The major contribution to the integral will come from around this value of ξ. We calculate $\bar{\xi}$, using for simplicity $\theta_0 = \pi/4$ and eliminating the angle dependence with the choice $\phi = \pi/2$:

$$e^{\lambda R_L \bar{\xi}} = \frac{\bar{\xi}}{(\Delta^2 + \bar{\xi}^2)^{3/2}}.$$

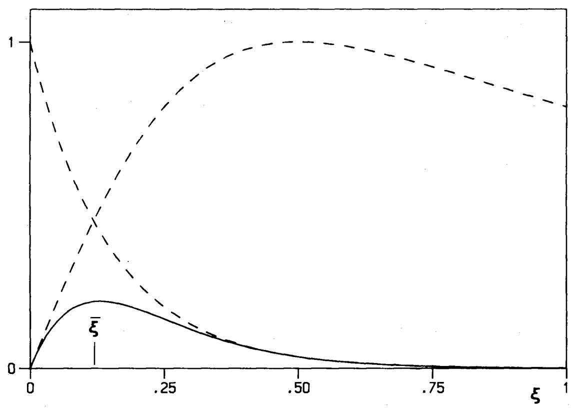

Fig. 3. Behaviour of the exponential and irrational function for $\Delta = 0.5$ in function f_1 in Eq. (15)

Let us suppose that $\bar{\xi} \ll 1$, as is reasonable (see Fig. 3); then

$$\bar{\xi} \simeq \frac{1}{\lambda R_L + 1/\Delta^3}.$$

We are looking for a solution far from the center; we may suppose that $1/\Delta^3 \ll \lambda R_L$, which is ~ 7; then, $r > 9$ kpc. This simplifies the preceding expression to $\bar{\xi} \simeq 1/\lambda R_L$. Consequently, the value for f_1 will be:

$$f_1 \simeq 2\pi \frac{e^{-1}(1/\lambda R_L)^2}{(\Delta^2 + (1/\lambda R_L)^2)^{3/2}} \simeq \frac{2\pi}{e} \frac{1}{(\lambda R_L)^2} \frac{1}{\Delta^3}. \tag{17}$$

The integral g_1 can be considered in a similar way. The corresponding maximum value of the integrand occurs at a value

$$\bar{\xi} \simeq \frac{1}{\lambda R_M + 1/\Phi^3}.$$

In this case, the two elements in the denominator of the preceding formula are of the same order. The estimate for g_1 gives:

$$g_1 \simeq 2\pi \frac{\bar{\xi}^2 e^{-\lambda R_M \bar{\xi}}}{(\Phi^2 + \bar{\xi}^2)^{3/2}}. \tag{18}$$

In calculating f_2 the angle dependence is not relevant for an estimate of the order of magnitude. It changes the result by a factor O(1).

The solution of the equation for $\bar{\xi}$

$$e^{\lambda R_L \bar{\xi}} = \frac{\bar{\xi}^2}{(\Delta^2 + \bar{\xi}^2)^{3/2}} \tag{19}$$

is more complicated. We assume that the maximum contribution to the integral comes from the same interval as that for f_1, giving

$$f_2 \simeq \frac{e^{-1}}{(\lambda R_L)^2 \Delta^3}. \tag{20}$$

In analogy, for g_2, we get:

$$g_2 \simeq \frac{\bar{\xi}^3 e^{-\lambda R_M \bar{\xi}}}{(\Phi^2 + \bar{\xi}^2)^{3/2}}, \tag{21}$$

where $\bar{\xi}$ comes from (19). Imposing the condition that $F_z = 0$, we get the following equation for r:

$$7215 \frac{Q_{\rm pr}}{a_{\rm nm}\delta} I_0 \Delta f_1 = \sigma_0 \Phi g_1 + \frac{M(r)}{r^2}. \tag{22}$$

For the optical and geometrical properties of dust grains, let us choose the following typical (extremal) sets of parameters.

	δ	$a_{\rm nm}$	$Q_{\rm pr}$(7000 K)	$Q_{\rm pr}/a_{\rm nm} \times \delta$
Astronomical silicate	3.3	50	0.131	$7.94\,10^{-4}$
Astronomical silicate	3.3	150	0.855	$1.73\,10^{-3}$
Graphite	2.26	20	0.334	$7.39\,10^{-3}$

The simple graphical solution of this equation is shown in Fig. 4. For the other component F_y we have, analogously:

$$7215 \frac{Q_{\rm pr}}{a_{\rm nm}\delta} (2^{-1/2} I_0 \Delta f_1 - I_0 f_2)$$
$$= 2^{-1/2} \sigma_0 \Phi g_1 - \sigma_0 g_2 + \frac{M(r)}{2^{1/2} r^2}. \tag{23}$$

The equilibrium radius in the y direction is, despite the rough approximation, essentially similar to the previous one (see Fig. 4). We can conclude that for silicate grains of radii 50–150 nm, there will be a large probability of trapping around 15 kpc, while graphite grains of 20 nm will have no equilibrium distance.

6. Qualitative considerations and observational aspects

In this section we raise the fundamental question: is there an observable effect produced by dust suspended out of the galactic disk?

First of all, we note that neither absorption nor emission effects are significant. Absorption will be obscured by absorption effects internal to the disk; the emission of dust confined in zones

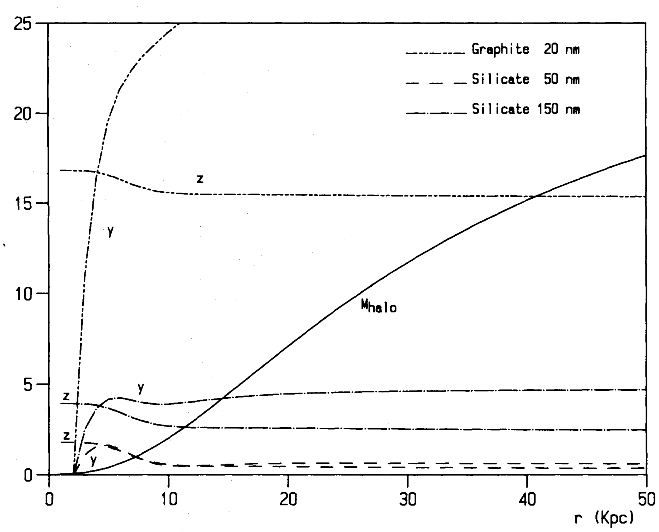

Fig. 4. Graphic solution for the equilibrium radii ($F = 0$) for NGC 3198 in the z and y directions for the grains listed in the table on this page. The intersection between $M(r)$ and the other y and z curves are the solutions of the Eqs. (22) and (23), respectively

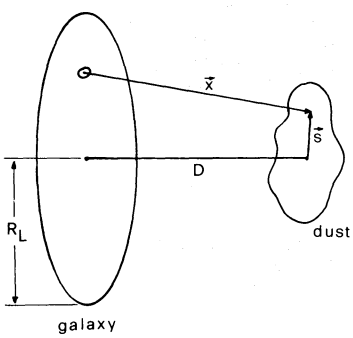

Fig. 5a. Halo dust lane geometry for the calculation of scattering efficiency

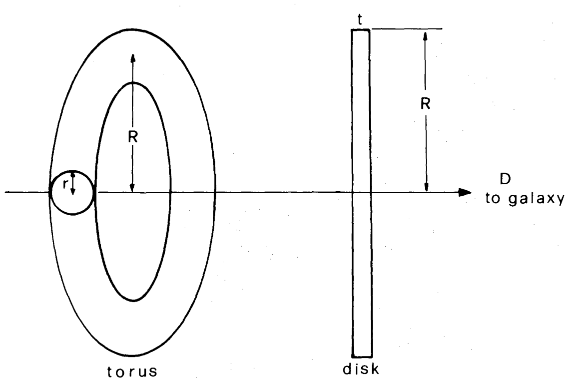

Fig. 5b. Halo dust lane geometries

external to the galactic disks may be quite small, because the dust temperature in these conditions must be not significantly greater than the background temperature (~ 5–10 K) and therefore invisible.

We must therefore look for scattering effects.[1] The geometry of the system is described in Fig. 5a. Without integrating the equation of motion, we assume that the distribution of dust is approximated by the following extreme configuration: ring (torus) or disk (Fig. 5b). This choice will help us to evaluate the importance of the geometrical factors in the result. The light scattered by grains per unit area, where N is the surface density of grains and Q_{sc} is the effective scattering cross section per unit area, is:

$$\frac{N\pi a^2 Q_{sc}}{4\pi}\int\frac{I(\rho)\rho\, d\rho\, d\phi}{|\boldsymbol{x}|^2} \tag{24}$$

[1] We like to introduce here a *methodological note*. Even though computers are large, powerful and inexpensive–relative to the useful results we can obtain from their use–they should not be used blindly. The economy of the research procedures (we are Galilean) and the laziness ("the great engine of world progress", P. Paolicchi 1986, private communication) which inhibits us to interpret hundreds of numerical results led us to consider first the question set at the beginning of this paragraph in a simple-minded way. It behoves one, before spending hours of CPU time, to try to justify the outcome, at least qualitatively.

As previously assumed, the surface brightness of the disk of a spiral galaxy is well approximated by the exponential function: $I(\rho) = I_0 e^{-\lambda\rho}$.

The integral may be written nondimensionally (as in Sect. 3):

$$I_0\int_0^{2\pi}\int_0^1 \frac{e^{-\lambda R_L \xi}\,\xi\, d\xi\, d\phi}{\dfrac{D^2+\rho^2}{R_L^2}+\xi^2-2\dfrac{\rho}{R_L}\xi\cos\phi} \equiv I_0 J, \tag{25}$$

schematically, for any geometry.

The ratio of light scattered by grains per unit area to the central surface brightness of the parent galaxy is

$$\Gamma = \frac{Na^2 Q_{sc}}{4} J \tag{26}$$

This is the quantity that can give the efficiency of scattering by dust grains on the light of the parent galaxy. Let us evaluate the terms in this expression. The surface density of grains N is related to the volume density n, for a torus and disk geometry by:

(a) torus geometry $\quad N = nr\frac{\pi}{2}$

(b) disk geometry $\quad N = 2nR\sin^2\theta\,(t \ll R)$,

where θ is the aperture angle of the disk. Assuming a homogeneous distribution:

$$n = f_x \frac{M_{dust}}{4/3\pi a^2 V\delta_g} \tag{27}$$

where M_{dust} is the dust mass in the galaxy, f_x the fraction of dust expelled and V the volume of the dust distribution.

Then we get:

$$\begin{aligned}&\text{(a)}\ n = \frac{f_x M_{dust}}{8/3\pi^3 Rr^2a^3\delta_g}\\ &\text{(b)}\ n = \frac{f_x M_{dust}}{4/3\pi^2 R^2 ta^3\delta_g}\end{aligned} \tag{28}$$

so that:

$$\begin{aligned}&\text{(a)}\ N = \frac{3}{16\pi^2}\frac{f_x M_{dust}}{Rra^3\delta_g}\\ &\text{(b)}\ N = \frac{3}{2\pi^2}\frac{f_x M_{dust}\sin^2\theta}{Rta^3\delta_g}\end{aligned} \tag{29}$$

The ratio Γ becomes:

$$\begin{aligned}&\text{(a)}\ \Gamma = \frac{3}{64\pi^2} J f_x Q_{sc}\frac{M_{dust}}{Ra\delta_g}\\ &\text{(b)}\ \Gamma = \frac{3}{8\pi^2} J f_x Q_{sc}\frac{M_{dust}\sin^2\theta}{Rta\delta_g}\end{aligned} \tag{30}$$

We give some simple quantitative estimates of Γ:

(a) Toroidal geometry. A typical estimate for M_{dust} is $\sim 10^{-3} M_{gal}$; adopting $M_{gal} = 10^{11} M_\odot$, we have $M_{dust} \sim 10^{41}$ g. We define the nondimensional parameters α, β, γ:

$$R = \alpha R_L, \qquad r = \beta R_L, \qquad a = \gamma\,\mu\text{m} \tag{31}$$

and chose $\delta_g = 3\ \text{g cm}^{-3}$. It is easy to show (as was done in Sect. 5 for similar integrals) that $1/15 \le J \le 1$. For example, if the exponential decrease is rapid, $\lambda R_L \gg 1$, so that the main contribution comes from the central region with $\xi_{max} \simeq 1/\lambda R_L$

and distance $|x|^2 \simeq R^2 + D^2$, and

$$J \simeq \frac{\pi}{\lambda^2(R^2+D^2)}. \tag{32}$$

If, as above, $R \simeq \alpha R_L$, $D \simeq R$, $\lambda \sim 3/R_L$, then $J \sim 1/6$. Then:

$$\Gamma \simeq \frac{1}{30}\frac{f_x Q_{sc}}{\alpha\beta\gamma}, \tag{33}$$

where α and β are related to the geometry of the dust torus, f_x with the efficiency of expulsion and dust confinment, Q_{sc} and γ with grains properties.

We discuss each of these parameters in detail:
1) α: (radius of torus in units of R_L), depends also on the nature and radius of grains, as is easy to understand looking at the figures of Sect. 7, but we may deduce from those figures that it is confined between 1/3 and 1. So a good estimate might be 1/2–1.
2) β: (radiud of torus section in units of R_L) This is likely to be less than α, so, as an estimate, we assume β in the range 1/10–1/3.
3) f_x: this parameter is strictly connected with the distribution of dust in the direction perpendicular to the galactic plane. Let us refer to the distribution known for the Milky Way. The IRAS data from 100 μm emission can be interpreted as generated by an exponential distribution with scale height 120 pc, similar to the H I distribution (Burton 1986). The dust filling factor is quite large: > 0.1. There might be a connection with the distribution of the stellar component of the galaxy. From the Bahcall and Soneira (1986) model, giant stars have a scale height of 250 pc, while for younger stars (O, B, A) the scale height is $\simeq$ 120 pc. The discussion of the distribution of dust internal to the disk will not be elaborated here, but we plan to come back to this, with a similar physical discussion, in the future. Let us suppose for the moment that the process of expelling the dust grains is efficient only for a small fraction of the matter present in such a phase, namely the part which is high enough above the plane, to be outside an isotropic distribution of stars. The simple way to estimate f_x is to evaluate the relative abundance of grains that are quite high above the disk. A schematic view of the vertical structure of the disk (Fig. 6) leads to the expression for f_x:

$$f_x = \frac{\int_{h_1}^{h_2} e^{-z/z_0}\,dz}{\int_{0}^{h_2} e^{-z/z_0}\,dz}, \tag{34}$$

where $z_0 = 120$ pc, h_1 and h_2 are the boundaries of the region where the expulsion process due to the nonisotropic radiation pressure is quite efficient. It is easy to calculate f_x for h_1 and h_2 near the outer edge (250 pc). We assume then $f_x \sim 10^{-2}$. So even using rather pessimistic values $\alpha = 1$, $\beta = 1/3$, $f_x = 10^{-2}$, we have

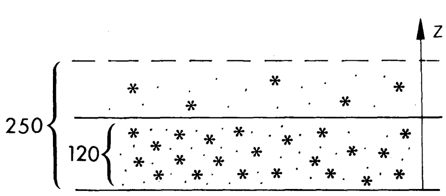

Fig. 6. Schematic vertical cut of the disk

$$\Gamma = 1\,10^{-3}\frac{Q_{sc}}{\gamma} \tag{35}$$

(b) Disk geometry. With similar assumptions and symbols as for the toroidal case we have

$$\Gamma = \frac{4}{15}\frac{f_x Q_{sc}\sin^2\theta}{\alpha\beta'\gamma}, \tag{36}$$

where β' is the disk thickness in units of R_L. As above $\alpha = 1$, $f_x \simeq 10^{-2}$, $\beta' = 1/3$, $\sin^2\theta = 1/2$, so that

$$\Gamma = \frac{2}{5}10^{-2}\frac{Q_{sc}}{\gamma}. \tag{37}$$

Q_{sc} is a function of γ and λ, the wavelength of the incoming radiation (hereafter measured in μm). As an estimate for Q_{sc}, we may adopt the choice by Rowan-Robinson (1980), who gives the following expression for grains with theoretical maximum efficiency that can reasonably represent the silicate-core ice-mantle grains:

$$Q_{sc} = 16\left(2\pi\frac{\gamma}{\lambda}\right)^4 \quad \text{if} \quad 2\pi\tfrac{\gamma}{\lambda} < \tfrac{1}{2}$$

$$Q_{sc} = 1 \quad \text{if} \quad 2\pi\tfrac{\gamma}{\lambda} > \tfrac{1}{2}.$$

For a wavelength of 4000 Å and a particle radius of 0.1 μm, we have

(a) $\Gamma = 10^{-2}$, (b) $\Gamma = 4\,10^{-2}$,

while for a wavelength of 2000 Å and $\gamma = 0.01$

(a) $\Gamma = 1.5\,10^{-2}$, (b) $\Gamma = 6.2\,10^{-2}$.

In all these cases, the ratio of scattered light to the galactic light is down by 3 to 5 mag: rather low, but not beyond the capabilities of present instrumental facilities. A strong support to this observational problem comes from the high polarization of the scattered light: about 20% for particles of 0.1 μm (Greenberg and Hanner, 1970).

The best subjects for observations are, then, edge-on galaxies, possibly quite isolated, where symmetrical lanes can be seen in the halo, providing double coincidences in the geometry and the polarization.

7. Computer analysis of the forces on silicate and graphite grains

We have performed an extended set of computer calculations of the gravitation and radiation pressure forces on graphite and astronomical silicate grains, under the following hypotheses:
1) The galaxy is NGC 3198.
2) Its radiation field has been modelled by a black body radiation field at temperatures 3000, 6000, 9000, 12000 K, with integrated value equal to the luminosity of the galaxy.
3) The grain radii are 10, 20, 50, 100, 150, 200, 250 nm.

Such a set of calculations gives a huge quantity of numbers. We have chosen to present the most interesting cases graphically. In the figures, we give the direction of the total force vector on a grain as a function of the polar galactic angle (from 5 to 90 degrees, in steps of 5 degrees) and of the galactocentric distance (5, 10, 20, 30, 40 and 50 kpc). To give an idea of the angular and radial dependence of the force value, for every galactocentric distance, the arrow lengths are proportional to the magnitude of the force; the maximum value of the force is written on the ordinate axis. This value is obtained from the parenthesized expressions in formula (14). Thus, to obtain the actual value of the force, multiply the values in the figures by $GmM_{\odot}/(\mathrm{pc})^2$.

Of the possible 56 graphs, we present here 12 illustrative examples. In general, one sees that the net force on graphite is such as to expel it from the galaxy. Figures 7a to 7d present some extreme cases, for small (10 nm) and large (200 nm) particles, and for reasonable values of the colour temperature of the galaxy (3000 and 6000 K). The generalized graphite expulsion is due to the large radiation pressure coefficient characteristic of this highly absorbing material. In particular, one sees that this expulsion property is largely independent of the colour temperature of the model galaxy.

The other figures present results for the astronomical silicate. This material shows many peculiar properties as far as the general galactic force is concerned. The graphs that we present are for a variety of grain sizes and for various galactic colour temperatures. We see that, in general, for all these grains there is a particular galactic zone where the gravitational and the radiative force can balance.

The first group of figures (Fig. 8a–d) applies to a grain of radius a = 100 nm for galactic colour temperature ranging from 3000 to 12000 K. The zone of stability is not present at the low temperature end and goes from a few kpc to 40–50 kpc with increasing galactic temperature. It is also clear that the difference

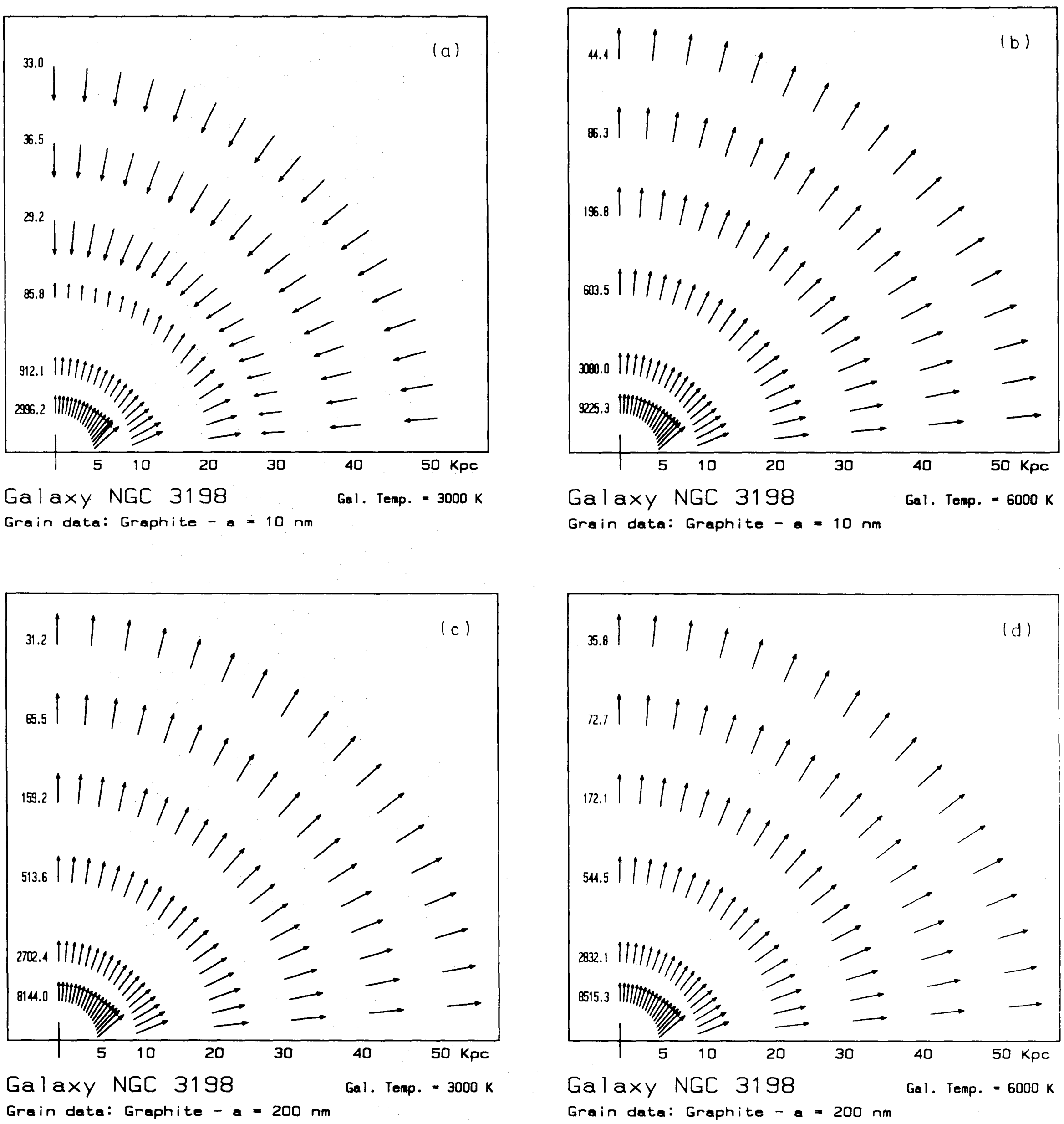

Fig. 7a–d. Angular and radial distribution of the forces on graphite grains. **a** a = 10 nm, T = 3000 K; **b** a = 10 nm, T = 6000 K; **c** a = 200 nm, T = 3000 K; **d** a = 200 nm, T = 6000 K

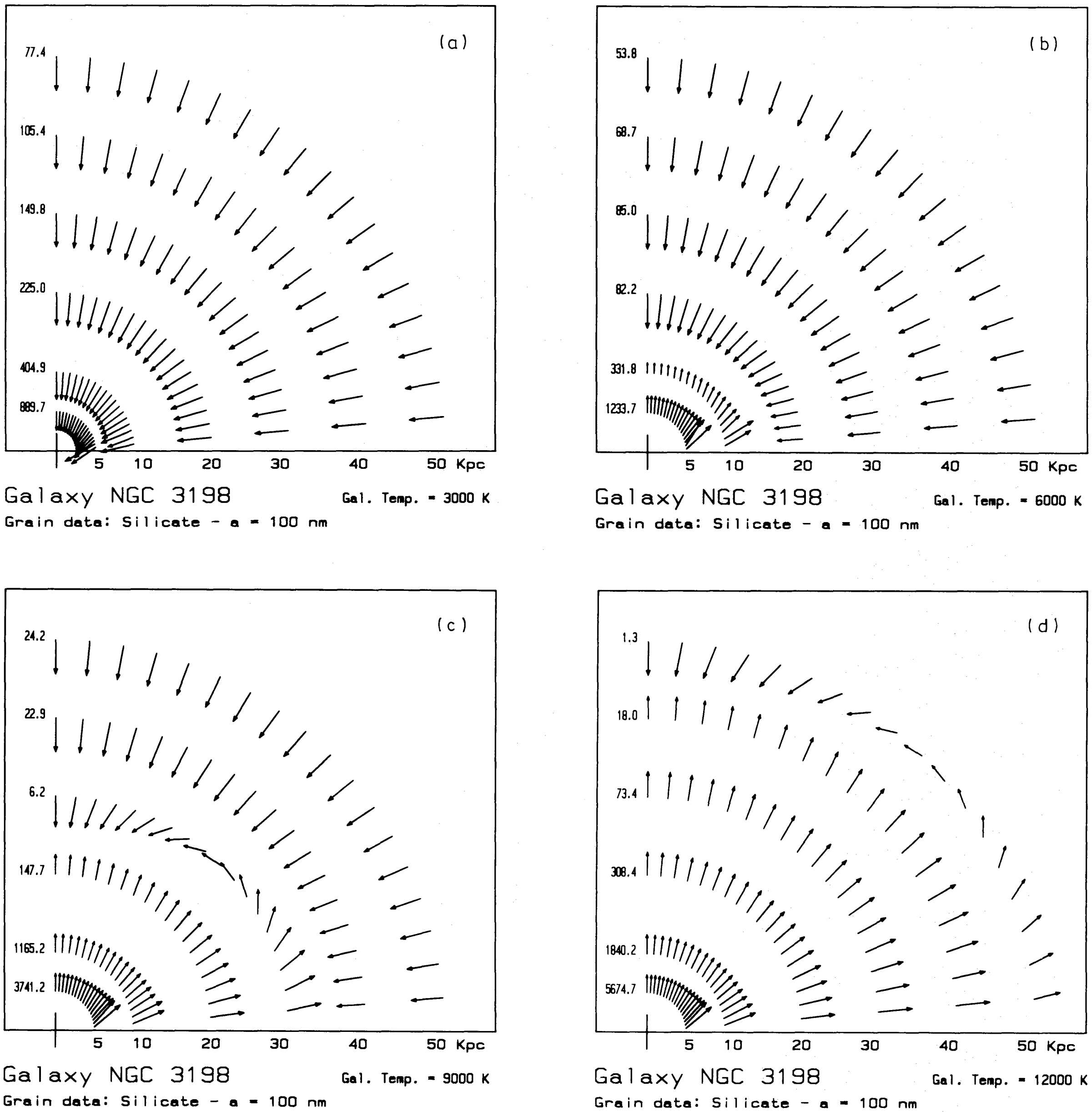

Fig. 8a–d

Fig. 8a–h. Angular and radial distribution of the forces on silicate grains. **a** $a = 100$ nm, $T = 3000$ K; **b** $a = 100$ nm, $T = 6000$ K; **c** $a = 100$ nm, $T = 9000$ K; **d** $a = 100$ nm, $T = 12000$ K; **e** $a = 10$ nm, $T = 6000$ K; **f** $a = 50$ nm, $T = 6000$ K; **g** $a = 150$ nm, $T = 6000$ K; **h** $a = 250$ nm, $T = 6000$ K

between the gravitational and luminous galactic profiles leads to a confining potential well whose form is consistent with the hypothesis of the presence of dust halos in galactic polar zones.

The second group of figures (Fig. 8e–h) shows the total force for fixed galactic colour temperature ($T_0 = 6000$ K) and for different grain radii ($a = 10$, 50, 150 and 250 nm). These figures show the expulsion and stable orbit effect of the force for particles of different radii.

8. Discussion and comparison with previous work

In 1972, Pecker published a paper in which he noted: "... il ne nous semble pas que l'evolution dynamique ... des gaz et poussieres qui ... composent le milieu interstellaire, air reçu un traitement suffisant". Today we may affirm that, at least as regards dust particles, Pecker's comment still has some validity, at least with regard to the galactic scale.

Only two papers by Pecker (1972, 1974) and one paper by Chiao and Wickramasinghe (1972) have taken up large scale dust motion. The connections and differences between our approach and the earlier ones require some discussion. In all cases, particle motions are considered far enough from stars to disregard any local effect (winds, etc.). Pecker (1972) considered, at first, the effect of individual stars of various spectral types on grains, ranging from 1 to 10^4 nm, varying the star spectral type (and consequently their effective temperature). The optical properties

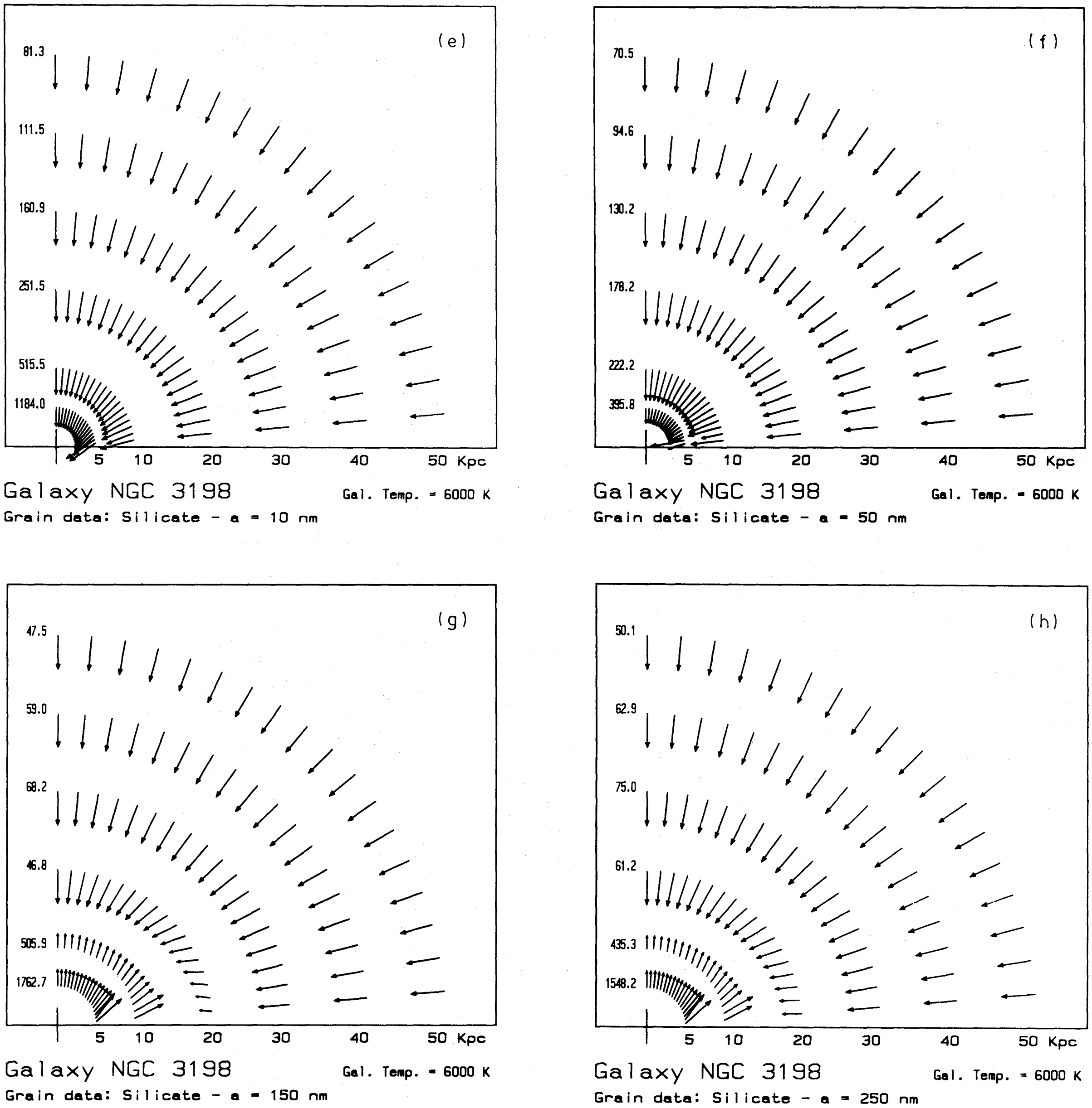

Fig. 8e–h

of the grains, that is their Q_{pr}, were considered in a rather qualitative way.

He concluded that grain size plays a larger role than its composition, resulting in a particularly efficient expulsion for grains with radii $\simeq 100$ nm; the early type stars (O5) can efficiently expel any grain along with hydrogen and carbon atoms. This conclusion can create serious problems for any model of the chemical evolution of galaxies which require an Initial Mass Function (IMF) with a larger number of massive stars at the beginning of the galaxy to provide a rapid enrichment of metals. The dynamical action of these very luminous stars might drastically reduce the quantity of metals produced in the early phase and change the ratio of element abundances.

The subsequent step in Pecker's calculation was the evaluation of the forces exercised by a 'synthetic' galaxy on dust particles. His model takes into account, schematically at least, the presence of "invisible matter" in the disk, as well as a distribution of visible matter and light in the disk.

The result is a generalized attraction of dust grains, but this is true for very high temperatures of the stars in the disk. Pecker thus concluded that the time variation of the ration M/L is a fundamental factor in determining the behaviour of grains, especially as regards the early phases of evolution of our galaxy.

This last aspect was also considered in a subsequent paper (Pecker 1974; in particular see Fig. 1). The real variation of M/L with time is indeed more complicated than the one assumed by Pecker: a large quantity of new data about the history of spiral galaxies is now at our disposal. The growth rate of the disk and the variation of star formation rate are the two parameters governing M/L. There is not yet a clear understanding of its history. Of particular interest for us are the conclusions of Pecker's second paper, which provided the motivations of this series of papers.

Chiao and Wickramasinghe (1972) studied the problem in a similar way, first in the interior of the disk, by calculating the contributions of single stars, with gravitation and radiation forces being calculated in a simple way. In the discussion of forces inside the disk, these authors correctly take into account the drag force due to gas clouds and the magnetic drift exerted on charged grains.

The ejection of grains from an entire spiral galaxy resulted in the expression:

$$\frac{F_{\rm rad}}{F_{\rm grav}} = \frac{7.84\,10^{-4}}{a\delta} \langle Q_{\rm pr} \rangle \left\langle \frac{L}{M} \right\rangle.$$

They concluded that the expulsion of dust grains is very efficient for spiral galaxies.

The fact that the conclusions of these authors are contradictory is a clear indication that, although the physics of this problem can be formulated very simply, the end result depends critically on the choice of parameters. This is the main motivation leading to our work: in the present paper we have limited our analysis to the static aspects of the forces: a prediction of the time scales for expulsion and confinement can be done only after a careful integration of the equations of motion (in preparation).

The systematic removal of graphite from the *upper* layers of the disk and the confinement of silicates in the halo have interesting consequences on various aspects of galactic evolution.

For example, the selective expulsion of some form of condensed matter may justify anomalies in the abundances of some elements, as well as suggesting that the extragalactic extinction corrections may be substantially different from a simple extrapolation of the adopted grain population in the disk.

Contamination of the disk diffuse matter by grains generated in external galaxies seems to be excluded, while on the other hand, the dust lanes observed in numerous elliptical galaxies (Bertola, 1987) may originate from the capture of the suspended dust during a low velocity crossing.

A further interesting aspect is related to the mass distribution in the halo: a positive observation of a dust concentration high above the disk may supply a new test on the amount of dark matter in galactic halos.

References

Bahcall, J.N., Soneira, R.M.: 1984, *Astrophys. J. Suppl.* Series **55**, 67

Bertola, F.: 1987, in *Structure and Dynamics of Elliptical Galaxies*, IAU Symposium 127, ed. T.D. Zeeuw, Reidel, Dordrecht

Burns, J.A., Lamy, P., Soter, S.: 1979, *Icarus* **40**, 1

Burstein, D., Rubin, V.C.: 1985, *Astrophys. J.* **297**, 423

Burton, W.B.: 1986, in *Proc. CI SIF Int. School of Physics "Enrico Fermi", Varenna*, eds. J.M. Greenberg, S. Aiello, Academic Press, New York

Chiao, R.Y., Wickramasinghe, N.C.: 1972, *Monthly Notices Roy. Astron. Soc.* **159**, 361

Draine, B.T., Lee, H.M.: 1984, *Astrophys. J.* **285**, 89

Draine, B.T., Salpeter, E.E.: 1979, *Astrophys. J.* **231**, 77

Greenberg, J.M., Chlewicki, G.: 1983, *Astrophys. J.* **272**, 563

Greenberg, J.M., Ferrini, F., Barsella, B., Aiello, S.: 1987, *Nature* **327**, 214

Greenberg, J.M., Hanner, M.S.: 1970, *Astrophys. J.* **161**, 947

Güsten, R., Metzger, R.G.: **1983,** *Vistas in Astronomy* **26**, 159

Hong, S.S., Greenberg, J.M.: 1980, *Astron. Astrophys.* **88**, 194

Mathis, J.S., Rumpl, W., Nordsiek, K.H.: 1977, *Astrophys. J.* **217**, 425

Mihalas, D., Binney, J.: 1981, in *Galactic Astronomy*, Freeman, San Francisco

Pecker, J.-C.: 1972, *Astron. Astrophys.* **18**, 253

Pecker, J.-C.: 1974, *Astron. Astrophys.* **35**, 7

Phillip, H.L.: 1977, *Phys. Rev.* **B16**, 2896

Rowan-Robinson, M.: 1980, *Astrophys. J. Suppl.* Series **44**, 403

Rudnicki, K.: 1986, in *Proc. of LXXXVI SIF Int. School of Physics "Enrico Fermi", "Cosmologia di Gamow"*, eds. F. Melchiorri, R. Ruffini, North-Holland, Amsterdam, p. 480

Shin, J., Hong, S.S.: 1987, *J. Korean Astron. Soc.* **20**, 1

Shull, J.M.: 1987, in *Interstellar Process*, eds. D.J. Hollenbach, H.A. Thronson Jr., Reidel, Dordrecht, p. 225

Tosatti, E., Bassani, F.: 1970, *Nuovo Cimento* **65B**, 161

van Albada, T.S., Bahcall, J.N., Begeman, K., Sancisi, R.: 1985, *Astrophys. J.* **295** 305

Wevers, B.M.H.R.: 1984, Ph.D. Thesis, Groningen University